

On the applicability of Kerker preconditioning scheme to the self-consistent density functional theory calculations of inhomogeneous systems

Yuzhi Zhou,^{1,2} Han Wang,^{2,3} Yu Liu,^{1,2} Xingyu Gao,^{1,2} and Haifeng Song^{1,2}

¹*LCP, Institute of Applied Physics and Computational Mathematics,
Beijing 100088, Peoples Republic of China*

²*Software Center for High Performance Numerical Simulation,
Chinese Academy of Engineering Physics,
Beijing 100088, Peoples Republic of China*

³*Institute of Applied Physics and Computational Mathematics,
Beijing 100088, Peoples Republic of China*

(Dated: February 13, 2020)

Abstract

Kerker preconditioner, which is based on the dielectric function of homogeneous electron gas, is designed to accelerate the self-consistent field (SCF) density functional theory (DFT) based total-energy calculations. However, question still remains regarding its applicability to the inhomogeneous systems. In this paper, we develop a generalized Kerker preconditioning scheme which captures the essence of the long-range screening behavior of inhomogeneous systems thus improve the convergence. The effectiveness and efficiency of this preconditioning model is shown by the convergence tests on long- z slabs of metals, insulators and metal-insulator contacts.

I. INTRODUCTION

Over the past few decades, the Kohn-Sham density functional theory (DFT) calculation [1, 2] has evolved into one of the most popular *ab initio* approaches for predicting the electronic structures and related properties of matters. The computational kernel of the Kohn-Sham DFT calculation is to solve a tangible nonlinear eigenvalue problem, replacing the original difficult many-body problem [2]. It is usually solved by the self-consistent field (SCF) iteration methods, which have proved to be quite reliable and efficient in most cases [3]. However, the well known "charge sloshing" problem is likely to occur in the SCF iterations as the dimension of the system gets large. The charge sloshing generally refers to the long-wavelength oscillations of the output charge density due to some small changes in the input density during the iterations, and results in a slow convergence or even divergence [3–5]. In some cases it might be referred to the oscillation between different local states of the d or f electrons [6]. In this work, we mainly concentrate on the discussion of the former situation.

For a fixed number of total atoms, the charge sloshing and poor SCF convergence are more prominent and exacerbated in the long- z slab systems, where one dimension of the unit cell is much longer than the other two's. On the other hand, investigating the properties of the surface and interface using DFT calculations has become one important subject in many scientific and technological fields, such as solid state physics, semiconductor processing, corrosion, and heterogeneous catalysis [7, 8]. The surface/interface is generally simulated by the long- z slab model with the periodic boundary condition. Especially when one comes to distinguish the properties between the bulk and the surface, a rather thick slab is needed to fully restore region with bulk-like properties. One example is the calculation of the band offsets at the heterojunction of semiconductors [9]. To get a quantitatively accurate band offset value, the lattice of both semiconductors must be extended far away from the contact region to restore bulk-like region, resulting in a very thick slab model. Similar example is the calculation of work function. Generally speaking, the slab calculation requires higher accuracy and more computational cost than typical bulk calculation. Effective and efficient mixing schemes are therefore needed to speed up the convergence of in the calculations of surface/interface investigations.

A practical mixing scheme in the modern DFT code generally takes into account two

aspects: (1) combining the results from previous iterations to build the input for next step; (2) Reflecting the dielectric response of the system (better known as "precondintioning"). For the first aspect, Pulay and Broyden-like schemes are well established and widely used [10, 11]. For the second aspect, Kerker in 1981 proposed that charge mixing could be preconditioned by a diagonal matrix in the reciprocal space. This matrix takes the form of inverse dielectric matrix derived from Thomas-Fermi model of homogeneous electron gas [12]. As pointed out in many work (and we will briefly visit it again in the next section), the preconditioning matrix should be an approximation to the dielectric function of the system [3, 13, 14]. In this sense, the Kerker preconditioner is ideal for simple metals such as Na and Al in which the conduction electrons behave like free electrons. Moreover, for most metallic systems, the Kerker preconditioner is a suitable preconditioner since it describes the dielectric responses at long wavelength limit fairly well. This observation then raises a natural question: Can Kerker preconditioning technique be applied to the non-metallic systems and hybrid systems of metal-insulator contact?

Many efforts have been made to develop effective preconditioning schemes to accommodate the inhomogeneity: Kresse *et al.* suggests that a lower bound can be added to the Kerker scheme to improve the convergence in the large insulating systems [3]. Raczkowski *et al.* use the Thomas-Fermi-von Weizsäcker equation to directly solve for the optimized mixing density in which process the full dielectric function is implicitly solved [13]; Shiihara *et al.* recast the Kerker preconditioning scheme in the real space for efficient SCF based real-space DFT calculations [15]; Lin and Yang further proposed an elliptic preconditioner in the real space to better accommodates the SCF calculations of large inhomogeneous systems [16]; Ho *et al.* [17], Sawamura *et al.* [18] and Anglade *et al.* [19] adopt similar preconditioning schemes in which the exact dielectric matrix is computed by the calculated Kohn-Sham orbitals.

Many of the above efforts focus on solving for the realistic dielectric response either explicitly or implicitly, which inevitably increase the computational cost. However, in practical, finding a good preconditioner does not necessarily mean finding the dielectric function as accurately as possible. Because in the context of SCF calculation, the total calculation time to reach the convergence is more of the concern. Spending much time in computing the accurate dielectric function and reaching the convergence in few steps might not be as efficient as using a much simpler preconditioner and reaching the convergence in maybe slightly more

steps.

In this paper, we focus on extending the applicability of the Kerker preconditioning model, which is based on a rather simple dielectric function model, i.e. the Thomas-Fermi screening model. To achieve this goal, we develop a modified Kerker preconditioning scheme that characterize the long range screening behavior of various inhomogeneous systems. Further we show that our preconditioning scheme indeed improve the convergence. For perfect insulating system, we introduce a threshold parameter to represent the incomplete screening behavior at small reciprocal lattice vector. With a proper setting of the threshold parameter, the SCF iterations can efficiently reach the convergence and seems independent on the system size. For metal-insulator hybrid systems and insulators containing metal-like defect states, the idea of the "effective" metal-like electrons is introduced to the module of the Thomas-Fermi wave vector in the original Kerker preconditioner. With the modified Kerker preconditioning scheme, we can achieve the SCF convergence within 30 iterations in calculating Au-MoS₂ hybrid slabs (with a cell parameter of 16 nm along z axis), saving about 40% of the SCF iteration steps compared to the original Kerker scheme. To achieve a fairly good SCF convergence with lack of *a priori* knowledge, we explore the a posteriori indicator to show whether the charge sloshing has been suppressed and to guide a reasonable parameter setting. Our methods require only small modifications based on the original Kerker scheme implemented in the modern DFT codes, but can be applied to a wide range of inhomogeneous systems with large dimensions.

This paper is organized as follows: In Section II, we will reformulate the Pulay mixing scheme to show the physical meaning of preconditioner for solving the fixed-point equation. In Section III, we will revisit the Thomas-Fermi and Resta screening models to extend the Kerker preconditioner to the non-metallic systems. In Section IV, the effectiveness and efficiency of our approach will be examined by several numerical examples. A further discussion on the essence of this preconditioning technique and a posteriori indicator will be given in Section V. Finally, some concluding remarks will be presented in the last section.

II. MATHEMATICAL FRAMEWORK

A. Simple mixing and preconditioning

Finding the solution of the Kohn-Sham equation where the output density $n^{\text{out}}(\mathbf{r})$ is equal to the input density $n^{\text{in}}(\mathbf{r})$ can be generalized to the following fixed point equation:

$$\mathbf{F}(\mathbf{x}) = \mathbf{x}, \quad (1)$$

\mathbf{x} denotes a vector in many dimensions, e.g. the density is expanded in the dimensions of a set of plane waves. This becomes a minimization problem for the norm of the residual $\|\mathbf{R}(\mathbf{x})\|$:

$$\mathbf{R}(\mathbf{x}) \equiv \mathbf{F}(\mathbf{x}) - \mathbf{x}. \quad (2)$$

The simplest method for seeking the solution of Eq. (1) is the fixed point iteration:

$$\mathbf{x}_{m+1} = \mathbf{F}(\mathbf{x}_m). \quad (3)$$

In the region where \mathbf{F} is a linear function of \mathbf{x} and \mathbf{x}^* is the solution of Eq' (1), we have

$$\mathbf{x}_{m+1} - \mathbf{x}^* = \left(\frac{\delta \mathbf{F}}{\delta \mathbf{x}} \right)^m (\mathbf{x}_1 - \mathbf{x}^*).$$

Therefore, a necessary condition that guarantees the convergence of the fixed point iteration is

$$\sigma \left(\frac{\delta \mathbf{F}}{\delta \mathbf{x}} \right) < 1,$$

where $\sigma(A)$ is the spectral radius of the operator (or matrix) A . However, in the Kohn-Sham density functional theory, the above condition is generally not satisfied [5].

However, the simple mixing can reach convergence as long as $\sigma \left(\frac{\delta \mathbf{F}}{\delta \mathbf{x}} \right)$ is bounded. The simple mixing scheme takes the form:

$$\mathbf{x}_{m+1} = \mathbf{x}_m + P \mathbf{R}(\mathbf{x}_m), \quad (4)$$

where P is the matrix whose size is equal to the number of basis functions. We define the Jacobian matrix:

$$J \equiv -\frac{\delta \mathbf{R}}{\delta \mathbf{x}} = I - \frac{\delta \mathbf{F}}{\delta \mathbf{x}}, \quad (5)$$

and denote its value at \mathbf{x}^* by J_* . When \mathbf{x}_m are sufficiently close to \mathbf{x}^* , the residual propagation of simple mixing Eq. (4) is given by:

$$\mathbf{R}(\mathbf{x}_{m+1}) \approx (I - J_* P) \mathbf{R}(\mathbf{x}_m). \quad (6)$$

In some literature [3, 5, 16], P is αI with α being a scalar parameter. Then it follows from Eq. (6) that the simple mixing will lead to convergence if:

$$\sigma(I - \alpha J_*) < 1. \quad (7)$$

If $\lambda(J_*)$ is an eigenvalue of J_* , then the inequality Eq. (7) indicates that:

$$\|1 - \alpha\lambda(J_*)\| < 1. \quad (8)$$

Note that $\lambda(J_*) > 0$ is referred to as the stability condition of the material in [20]. And it holds in most cases according to the analysis given in [5]. Consequently, Eq. (8) implies that:

$$0 < \alpha < \frac{2}{\lambda(J_*)}. \quad (9)$$

When $\lambda(J_*)$ is bounded, it is always possible to find a parameter α to ensure the convergence of the simple mixing scheme. Nevertheless, $\lambda(J_*)$ can become very large in practice, especially in the case of metallic systems with large dimensions, which makes the convergence of the simple mixing extremely slow. Therefore it is desirable to construct effective preconditioning matrix P in Eq. (4) to speed up the convergence.

Here we want to explicitly show that in the context of the charge mixing, the Jacobian matrix J is just the charge dielectric response function, which describes the charge response to an external charge perturbation. Replacing the \mathbf{x}_m in Eq. (4) with charge density \mathbf{n}_m , we have:

$$\mathbf{n}_{m+1} = \mathbf{n}_m + P \cdot \mathbf{R}(\mathbf{n}_m) \quad (10)$$

For $\mathbf{R}(\mathbf{n}_m)$, we could expand it to the linear order as:

$$\mathbf{R}(\mathbf{n}) = \mathbf{R}(\mathbf{n}_m) - J \cdot (\mathbf{n} - \mathbf{n}_m) \quad (11)$$

The J in the above equation is just the Jacobian matrix defined earlier in Eq. (5). We always want to achieve as much self consistency as possible in the next step, such that $\mathbf{R}(\mathbf{n}_{m+1}) \approx 0$. Plugging this into Eq. (11), we have:

$$\mathbf{n}_{m+1} = \mathbf{n}_m + J^{-1} \cdot \mathbf{R}(\mathbf{n}_m) \quad (12)$$

Comparing this equation with Eq. (10), we see that $P = J^{-1}$. The problem then becomes finding a good approximation of the Jacobian matrix J . To prove that J has the physical

meaning of charge dielectric function, we follow Vanderbilt and Louie's procedure in Ref. [14]:

$$\mathbf{V}_{m+1} \approx \mathbf{V}_m + U \cdot (\mathbf{n}_{m+1} - \mathbf{n}_m) \quad (13)$$

where the matrix U describe the change in the potential due to a change in the charge density. As a result, the output charge density is given by:

$$\mathbf{n}_{m+1}^{\text{out}} \approx \mathbf{n}_m^{\text{out}} + \chi \cdot (\mathbf{V}_{m+1} - \mathbf{V}_m) \quad (14)$$

where χ is just the electric susceptibility matrix, describing the change in the output charge density due to a change in the potential. Combining Eqs. (10), (11), (13) and (14), we arrive at:

$$J = I - \chi \cdot U \quad (15)$$

J is often called as the dielectric matrix. According to Vanderbilt and Louie [14], J^{-1} is the *charge* dielectric response function which describes the fluctuation in the total charge due to a perturbation from external charge. Reversing the order of Eqs. (13) and (14) and adopting the potential mixing, we can also obtain a dielectric response function $(I - U \cdot \chi)^{-1}$ which describes the potential response to an external potential perturbation. Note that the order of the matrix product matters and generally the *charge* dielectric response function and *potential* dielectric response function are different but closely related.

Also note that this derivation is independent of the basis set, which could either be a plane-wave basis set or atomic-orbital basis set. As mentioned before, a good preconditioning scheme is to mimic the charge dielectric response in the charge mixing at a reasonable computational cost. A detailed discussion of the Kerker preconditioning model will be presented in the next section.

B. Pulay mixing scheme

Instead of using vector \mathbf{x}_m only from last step in (4), we could minimize the norm of the residual $\|\mathbf{R}(\mathbf{x})\|$ using the best possible combination of the \mathbf{x}_m from all previous steps. This is the idea behind the technique called Direct Inversion in the Iterative Subspace (DIIS). The technique is originally developed by Pulay to accelerate the Hartree-Fock calculation [10]. Hence it is often referred to as Pulay mixing in the condensed matter physics community.

In the Pulay's original work [10], the optimal approximation to the next vector is presented as:

$$\mathbf{x}_{m+1} = \sum_{i=0}^{l-1} a_{m-i} \mathbf{x}_{m-i}, \quad (16)$$

where $l = \min\{m, L\}$ with $m > 0$ and L being the maximal dimension of the subspace. We choose the coefficients a_{m-i} in Eq. (16) through solving the constraint optimization problem:

$$\begin{cases} \min_{\{a_{m-i}\}} \left\| \mathbf{R} \left(\sum_{i=0}^{l-1} a_{m-i} \mathbf{x}_{m-i} \right) \right\|^2 \\ \text{s.t. } \sum_{i=0}^{l-1} a_{m-i} = 1, \end{cases} \quad (17)$$

where $\|\cdot\|$ is some norm derived from the inner product $\langle \cdot \rangle$. To improve the numerical stability [4], we construct the next input vector as

$$\mathbf{x}_{m+1} = \mathbf{x}_m - \sum_{i=1}^{l-1} b_{m-i} \delta \mathbf{x}_{m-i}, \quad (18)$$

where $\delta \mathbf{x}_{m-i} = \mathbf{x}_{m-i+1} - \mathbf{x}_{m-i}$. Then the coefficients b_{m-i} are determined by solving the unconstraint optimization problem:

$$\min_{\{b_{m-i}\}} \left\| \mathbf{R} \left(\mathbf{x}_m - \sum_{i=1}^{l-1} b_{m-i} \delta \mathbf{x}_{m-i} \right) \right\|^2 \quad (19)$$

When the vectors \mathbf{x}_{m-i} are all sufficiently close to the solution of Eq. (1), the linearity of the residual near the solution leads to:

$$\begin{aligned} & \frac{1}{2} \frac{\partial}{\partial b_{m-i}} \langle \mathbf{R}(\mathbf{x}_{m+1}) \mid \mathbf{R}(\mathbf{x}_{m+1}) \rangle \\ &= - \langle \delta \mathbf{R}_{m-i} \mid \mathbf{R}(\mathbf{x}_m) \rangle + \sum_{j=1}^{l-1} b_{m-j} \langle \delta \mathbf{R}_{m-i} \mid \delta \mathbf{R}_{m-j} \rangle. \end{aligned} \quad (20)$$

Let

$$A_{ij} = \langle \delta \mathbf{R}_{m-i} \mid \delta \mathbf{R}_{m-j} \rangle, \quad i, j = 1, 2, \dots, l-1, \quad (21)$$

and the solution of Eq. (19) can be written as:

$$\mathbf{b}_{m-i} = \sum_{j=1}^{l-1} (A^{-1})_{ij} \langle \delta \mathbf{R}_{m-j} \mid \mathbf{R}(\mathbf{x}_m) \rangle. \quad (22)$$

Inserting Eq. (18) into Eq. (4), we obtain the general form of Pulay's method:

$$\mathbf{x}_{m+1} = \mathbf{x}_m + P \mathbf{R}(\mathbf{x}_m) - \sum_{j=1}^{l-1} \left[\sum_{i=1}^{l-1} (A^{-1})_{ij} (\delta \mathbf{x}_{m-i} + P \delta \mathbf{R}_{m-i}) \right] \langle \delta \mathbf{R}_{m-j} \mid \mathbf{R}(\mathbf{x}_m) \rangle \quad (23)$$

An alternative way to derive Pulay method is taking it as the special case of the Broyden's method [21]. In the Broyden's second method, a sequence of low-rank modifications are made to some initial guess of the inverse of the Jacobian matrix Eq. (5) near the solution of Eq. (1). The recursive formula [6, 22] can be derived from the following constrained optimization problem:

$$\begin{cases} \min_H \frac{1}{2} \|H - H_{m-1}\|_F^2 \\ \text{s.t. } HY_{m-1} = -S_{m-1}, \end{cases} \quad (24)$$

where H_{m-1} is the approximation to the inverse Jacobian in the $(m-1)$ th Broyden update, S_{m-1} and Y_{m-1} are respectively defined as:

$$\begin{aligned} S_{m-1} &= (\delta \mathbf{x}_{m-1}, \dots, \delta \mathbf{x}_{m-l+1}), \\ Y_{m-1} &= (\delta \mathbf{R}_{m-1}, \dots, \delta \mathbf{R}_{m-l+1}). \end{aligned} \quad (25)$$

It will be later proved in the appendix that the solution to Eq. (24) is:

$$H_m = H_{m-1} - (S_{m-1} + H_{m-1}Y_{m-1}) (Y_{m-1}^T Y_{m-1})^{-1} Y_{m-1}^T. \quad (26)$$

We arrive at Pulay mixing scheme by fixing the H_{m-1} in Eq. (26) to the initial guess H_1 of the inverse Jacobian:

$$H_m = H_1 - (S_{m-1} + H_1 Y_{m-1}) (Y_{m-1}^T Y_{m-1})^{-1} Y_{m-1}^T. \quad (27)$$

Then one can follow the quasi Newton approach to generate the next vector:

$$\mathbf{x}_{m+1} = \mathbf{x}_m + H_m \mathbf{R}(\mathbf{x}_m) \quad (28)$$

$$= \mathbf{x}_m + H_1 \mathbf{R}(\mathbf{x}_m) - (S_{m-1} + H_1 Y_{m-1}) (Y_{m-1}^T Y_{m-1})^{-1} Y_{m-1}^T \mathbf{R}(\mathbf{x}_m). \quad (29)$$

Note that it is natural to take the l_2 norm in Eq. (17) or (19) with plane wave basis. Then it is obvious that Eq. (29) is the matrix representation of Eq. (23).

We also comment that the construction of H_1 in Eq. (29) is crucial for accelerating the convergence since it can work as a preconditioner for the simple mixing Eq. (4). It is implied by Eq. (7) that preconditioning would be effective if H_1 is a good guess of the inverse Jacobian near the solution of Eq. (1). Under the Pulay mixing scheme, we focus our discussion on the Kerker preconditioning model and appropriate choices of parameters in the model.

III. PRECONDITIONING MODEL

A. Thomas-Fermi screening model

The Thomas-Fermi screening model is the foundation for the Kerker preconditioner, and many other preconditioning schemes as well. In this section, the derivation of the Thomas-Fermi screening model, i.e. the dielectric response function of the homogeneous electron gas, will first be given. In what follows, the implications of this screening model on the convergence behavior and Kerker preconditioning model will then be discussed in detail.

Consider an external defect charge (or some small perturbation in the charge density) being introduced into a homogeneous electron gas. The external potential then solely arises from the external charge and satisfies Poisson's equation:

$$-\nabla^2 V_{ext} = 4\pi n_{ext}(\mathbf{r}) \quad (30)$$

The external charge induces a cloud of screening electrons, resulting in a redistribution of the total potential and charge density. Similarly, we have:

$$-\nabla^2 V_{tot} = 4\pi n_{tot}(\mathbf{r}) \quad (31)$$

The difference between the total charge density and external charge density gives the induced charge density n_{ind} . One could assume that V_{tot} and V_{ext} are linearly related through the relation [23]:

$$V_{ext}(\mathbf{r}) = \int d\mathbf{r}' \varepsilon(\mathbf{r}, \mathbf{r}') V_{tot}(\mathbf{r}') \quad (32)$$

In the homogeneous electron gas, the dielectric matrix ε would only depends on the distance between the \mathbf{r} and \mathbf{r}' . Thus Eq. (32) becomes:

$$V_{ext}(\mathbf{r}) = \int d\mathbf{r}' \varepsilon(\mathbf{r} - \mathbf{r}') V_{tot}(\mathbf{r}') \quad (33)$$

Under the Fourier transform, we have the following relation for their Fourier components:

$$V_{ext}(\mathbf{q}) = \varepsilon(\mathbf{q}) V_{tot}(\mathbf{q}) \quad (34)$$

If the perturbation is weak and slow-varying in space (which is probably a good approximation near the self consistency), the induced charge density n_{ind} and the total potential V_{tot} are linearly linked by:

$$n_{ind}(\mathbf{q}) = \chi(\mathbf{q}) V_{tot}(\mathbf{q}) \quad (35)$$

We note that this relation shares the same spirit with Eq. (14). The Fourier transforms of the Poisson Eqs. (30) and (31) are:

$$\mathbf{q}^2 V_{ext}(\mathbf{q}) = 4\pi n_{ext}(\mathbf{q}) \quad (36)$$

$$\mathbf{q}^2 V_{tot}(\mathbf{q}) = 4\pi n_{tot}(\mathbf{q}) \quad (37)$$

Combining Eqs. (34), (35), (36) and (37), we have the relation between ε and χ :

$$\varepsilon(\mathbf{q}) = 1 - 4\pi \frac{\chi(\mathbf{q})}{\mathbf{q}^2} \quad (38)$$

Note that this is consistent with the general form given in Eq. (15). The dielectric matrix ε (or J in the context of previous section) is diagonalized due to the homogeneity of the system and can be seen as a function of \mathbf{q} . Now we focus on the calculation of the quantity $\chi(\mathbf{q})$. The induced charge density is the difference between systems with and without the external potential:

$$n_{ind}(\mathbf{r}) = -e[N(\mu + eV(\mathbf{r})) - N(\mu)] \quad (39)$$

where the electron number density N as a function of chemical potential μ is given by the Fermi-Dirac distribution and dispersion relation of the free electron gas:

$$N(\mu) = \int \frac{d\mathbf{k}}{4\pi^3} \frac{1}{\exp[\beta(\frac{\hbar^2 \mathbf{k}^2}{2m_e} - \mu)] + 1} \quad (40)$$

Based on the assumption that the external potential is weak and slow-varying in space, we could expand Eq. (39) near the electron chemical potential μ (or the Fermi energy ε_F) to the first order as:

$$n_{ind}(\mathbf{r}) = -e^2 \frac{\delta N}{\delta \mu} V(\mathbf{r}) \quad (41)$$

where the quantity $\frac{\delta N}{\delta \mu}$ is proportional to the number of states in the vicinity of the electronic chemical potential or Fermi level. Comparing Eqs. (41) and (35), we have:

$$\chi(\mathbf{q}) = -e^2 \frac{\delta N}{\delta \mu} \quad (42)$$

Thus, Eq. (38) now becomes:

$$\varepsilon(\mathbf{q}) = 1 + \frac{k_{TF}^2}{\mathbf{q}^2} \quad (43)$$

This is the dielectric function of the Thomas-Fermi screening model [43]. The Thomas-Fermi vector k_{TF} is defined through:

$$k_{TF}^2 = 4\pi e^2 \frac{\delta N}{\delta \mu} \quad (44)$$

Since the preconditioner is the inverse of the dielectric function, we now have a preconditioner that is based on this screening model:

$$H_1^{TF}(\mathbf{q}) = \frac{\mathbf{q}^2}{\mathbf{q}^2 + k_{TF}^2} \quad (45)$$

This is just the form of the Kerker preconditioner [3, 12, 16]. We would like to remark few things regarding the Thomas-Fermi screening model with its implication to SCF loop and Kerker preconditioner:

- a)** According to Eq. (43), at small \mathbf{q} or long wavelength, the dielectric function diverges quadratically. Assume a metallic system contains small \mathbf{q} 's. Then in the SCF loop, changes in the charge density will cause large changes in the potential (or more precisely, the Hartree potential) at long range. This, in turn, results in large and long-range changes in the output charge density, known as the "charge sloshing", thus causes the convergence hard to achieve. Such convergence issue is more prominent in the long-z metallic slab systems in which one dimension of the cell is much larger than the rest two. Therefore we focus our numerical tests on the slab systems.
- b)** The contribution from the exchange-correlation potential is neglected in the derivation. The exchange-correlation potential value, under the local density approximation (LDA) or generalized gradient approximation (GGA), depends on the local charge density (plus its derivatives in the case of GGA). In the long wavelength limit, this type of local potential is much smaller in magnitude compared to the Coulomb potential, which causes the $1/\mathbf{q}^2$ divergence at small \mathbf{q} . In this sense, the Thomas-Fermi screening as well as the Kerker preconditioning model are getting the correct behavior at the long wavelength limit. However, we lose some details of responses especially at larger \mathbf{q} by neglecting the effect from the exchange-correlation potential. Based on our numerical results, we believe predicting a (qualitatively) correct behavior of the preconditioner at small \mathbf{q} is the key part for improving the convergence.
- c)** Even though the dielectric function in Eq. (43) is mounted on the homogeneous electron gas, it still manifests an important feature of the electron screening in the metallic systems. As mentioned above, $\frac{\delta N}{\delta \mu}$ has the physical meaning of the number of the states in the vicinity of (below and above) the Fermi level. We can interpret this as: the electrons near the Fermi level are actively involved in screening since they can adjust themselves to higher unoccupied states to accommodate the change in the potential. On the other hand, deeper electrons

are limited by the high excitation energy or Pauli exclusion principle. This observation is somehow independent of the band structures of the system.

d) Following the above point, we further estimate the relation between the electron density and the parameter k_{TF} under the assumption of homogeneous electron gas. Since $\frac{\delta N}{\delta \mu}$ can be approximated by the number of states at the Fermi level, we can write k_{TF} as:

$$k_{TF}^2 \approx 4\pi e^2 N(\varepsilon_F) = \frac{4(3\pi^2 n_0)^{1/3}}{a_B \pi} \quad (46)$$

where a_B is the Bohr radius and n_0 is the total free electron density in the system:

$$a_B = \hbar^2/(me^2) \approx 0.53 \text{ \AA} \quad (47)$$

Plugging in numbers, we have the following relation:

$$k_{TF} \approx 2\left(\frac{n_0}{a_B^3}\right)^{1/6} \quad (48)$$

In a typical metal, $n_0 \approx 10^{23} \text{ cm}^{-3}$. Therefore, $k_{TF} \approx 1 \sim 2 \text{ \AA}^{-1}$. This is also the default value range used for most Kerker preconditioner in the calculations. As shown later in our examples, Eq. (48) could offer us guide to parameterized the k_{TF} and facilitates the convergence of the metal-insulator hybrid systems and insulating systems with metal-like defect states.

B. Resta screening model

The Thomas-Fermi screening model is more appropriate in describing the screening effect in the metallic system. Resta revised the boundary condition of the previous Poisson equation Eq. (31) and derived the screening model for semiconductors and insulators [24]. Rather than being completely screened at the long range in the metallic system, the potential is only partially screened beyond some screening length in the insulators. This is characterized by the static dielectric constant $\varepsilon(0)$:

$$V(\mathbf{r}) = -\frac{Z}{\varepsilon(0)r}, \quad r \geq R_s \quad (49)$$

Where R_s is the screening length which is generally on the order of the lattice constants. According to Resta, the relation between the screening length and the static dielectric constant is given by:

$$\varepsilon(0) = \frac{\sinh(q_0 R_s)}{q_0 R_s} \quad (50)$$

where q_0 is a constant related to the valence electron Fermi momentum k_F :

$$q_0 = (4k_F/\pi)^{1/2} \quad (51)$$

with k_F related to the average valence electron density n_0 by:

$$k_F = (3\pi n_0)^{1/3} \quad (52)$$

Under the atomic unit, q_0 is in the unit of 1 over distance. The dielectric function can be written as follow:

$$\varepsilon(\mathbf{q}) = \frac{q_0^2 + \mathbf{q}^2}{\frac{q_0^2 \sin(|\mathbf{q}|R_s)}{\varepsilon(0)|\mathbf{q}|R_s} + \mathbf{q}^2} \quad (53)$$

The three material parameters q_0 , R_s and $\varepsilon(0)$ in the above equation are related by Eq. (50) thus only two are needed for the input. The static dielectric constant $\varepsilon(0)$ and Fermi momentum related quantity q_0 can be extracted from the experimental data. In Resta's original paper, he offered the input parameters for Diamond, Silicon and Germanium in his original paper. He further showed that the Resta's dielectric functions for these materials are in close agreement with others derived from Penn-model results of Srinivasan [25, 26] and RPA calculations of Walter and Cohen [27]. However, the dielectric function he proposed is much simpler in the expression compared with others. Later on, Shajan and Mahadevan [28] used Resta's model to calculate the dielectric function of many binary semiconductors, such as GaAs, InP, ZnS, etc. Their results are found to be in excellent agreement with those calculated by the empirical pseudopotential method [29].

Here, we proposed the Resta's preconditioner which is based on Resta's model has the following form:

$$H_1^{Res}(\mathbf{q}) = \frac{\frac{q_0^2 \sin(|\mathbf{q}|R_s)}{\varepsilon(0)|\mathbf{q}|R_s} + \mathbf{q}^2}{q_0^2 + \mathbf{q}^2} \quad (54)$$

It is instructive to compare this preconditioner with Kerker preconditioner. The two preconditioners are plotted as the function of \mathbf{q} in Fig. 1. For Kerker preconditioner, the k_{TF} is chosen to be 1, in the unit of \AA^{-1} . For the Resta preconditioner, the static dielectric constant is chosen to be 6.5. For many semiconductors and insulators, this value falls into the range of $5 \sim 15$. The q_0 is chosen to be 1\AA^{-1} and the screening length is 4\AA , accordingly. These values are about the typical inputs for all binary semiconductors studied in [28]. From Fig.1, it is helpful to point out the following points:

a) At some \mathbf{q} values slightly below 1, the two curves start to merge. At relatively large \mathbf{q} ,

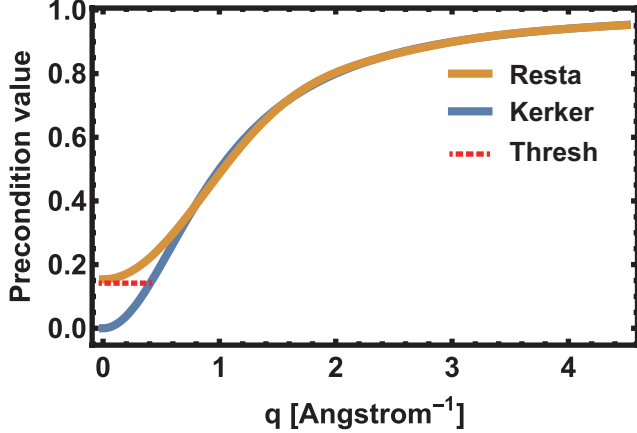


FIG. 1: (color online) The preconditioning models as a function of reciprocal vector \mathbf{q} . A threshold parameter can be added to the Kerker preconditioner to simulate the small \mathbf{q} behavior of the insulating systems.

they all converge to 1. This means the dielectric responses of metallic and insulating systems are the same at the short wavelength limit. This behavior, reflected in the preconditioners, leads to a simple mixing scheme for the large \mathbf{q} components.

b) The essential difference between the Kerker preconditioner and Resta preconditioner (and screening model as well) happens at small \mathbf{q} limit. For the Kerker preconditioner, as we have discussed in the previous section, it goes to zero quadratically. While for the Resta preconditioner, it goes to a finite value at \mathbf{q} equals zero and this value is just $1/\varepsilon(0)$. This represents the incomplete screening in the insulating systems due to a lack of conducting electrons. We also note if a nominal insulating system contains metal-like defect states (in other words there is an incompletely filled defect states), Resta preconditioner does not offer too much help in speeding up the convergence.

c) In practical, if one does not want to switch between the two preconditioning models when calculating different systems, a threshold can be added to the Kerker preconditioner to mimic the behavior of the Resta preconditioner at the small \mathbf{q} 's, as shown by the dashed line in the Fig. 1. Now the modified Kerker preconditioner has the form:

$$H_1^{TF'}(\mathbf{q}) = \max(a_0, \frac{\mathbf{q}^2}{\mathbf{q}^2 + k_{TF}^2}) \quad (55)$$

In the modified Kerker preconditioner, it will move part of the curve that is below a_0 to a_0 . This action restores the behavior of the screening effect in the insulating systems. In the code, the threshold parameter a_0 is set with a linear mixing parameter α multiplying the

preconditioner.

$$H_1^{TF''}(\mathbf{q}) = \max(a_0, \alpha \frac{\mathbf{q}^2}{\mathbf{q}^2 + k_{TF}^2}) \quad (56)$$

Accordingly, the optimal a_0 should be equal to $\alpha/\varepsilon(0)$. This modification extended the applicability of the Kerker preconditioner.

IV. NUMERICAL EXAMPLES

We have performed the convergence tests on various systems using the in-house code CESSP [30, 31] under the infrastructure of JASMIN [32]. The exchange and correlation energy is described by the generalized gradient approximation proposed by Perdew, Burke, and Ernzerhof [33]. Electron-ion interactions are treated with projector augmented wave potentials [34]. The first 5 steps of the iteration take the Blocked Davison scheme where no charge mixing takes place [35]. The following steps take the RMM-DIIS scheme [3]. The mixing parameter α is set to 0.4 in all calculations with different preconditioners. The convergence criterion for self-consistent field loop is 1×10^{-6} eV, which is a good enough criterion for practical slab system calculations. When constructing the slab models, we always include at least 20 Å of vacuum layer, which is used to exclude the spurious interaction between surfaces under the periodic boundary condition. Along the x and y directions the cells in all calculations are kept as primitive cell.

A. Au slab: the metallic system

The first system is the $\{111\}$ Au slab. We have constructed three Au slab systems with 14, 33 and 54 layer of Au $\{111\}$ planes, corresponding to a cell parameter of 5, 11 and 15 nm along the direction normal to Au $\{111\}$ surface, respectively. A $12 \times 12 \times 1$ k-point grid is used to sample the Brillouin zone. The cutoff energy is chosen to be 350 eV. Here, the Kerker preconditioner with no threshold parameter a_0 (referred as "original Kerker preconditioner") has been used to speed up the convergence. The k_{TF} has been set to 1 in the unit of Å⁻¹. The number of iterations to reach the convergence is listed in Table I.

We further note that using the simple mixing scheme cannot reach convergence within 120 steps for all three slabs. Thus the Kerker preconditioner does significantly improve the convergence for the long- z Au systems. In addition, the number of steps from Kerker

TABLE I: The number of convergence steps in the Au slab systems using original Kerker preconditioner.

Number of Au layers	Total slab thickness [nm]	Number of steps
14	5	27
36	11	32
54	15	31

preconditioner is weakly dependent on the size of the system, which is also an indication that the charge sloshing has been suppressed. As we have stated in the previous section, the charge sloshing phenomenon is a reflection of the quadratical divergence of the dielectric function at $\mathbf{q} \rightarrow 0$ limit. The Thomas-Fermi model and the Kerker preconditioner are getting this behavior right, even though the free electron gas model is not a good approximation for Au as well as many realistic metallic systems.

B. MoS₂: the layered insulating system

Secondly, we have studied the convergence of the layered insulating system: MoS₂. Two slab systems with 10 and 20 layers of MoS₂, corresponding to a cell parameter of 8 nm and 16 nm, have been constructed. The MoS₂ layers have been stacked in the same fashion as those in the bulk MoS₂. A $6 \times 6 \times 1$ k-point grid has been used to sample the Brillouin zone. The cutoff energy is 450 eV. Both Kerker and Resta preconditioners have been tested on the MoS₂ slab systems.

For the Resta preconditioner, we need the static dielectric constant and screening length as input parameters. We find the reported value of the average static elastic constant of MoS₂ varying in literature [36–39]. It is also found that this value depends on the number of MoS₂ layers. However, they all fall into the range of 5 ~ 15. Thus we have used three static dielectric constants 5, 10 and 15, in the Resta preconditioner. The screening length R_s has been set to 3.5 which is close to the lattice constants. The q_0 in the Resta model is then calculated by Eq. (50).

For the Kerker preconditioner, we adopt both the original and modified Kerker preconditioners. For both preconditioners, the Thomas-Fermi vector k_{TF} has been set to 1 Å⁻¹. For

the modified Kerker preconditioner, we have chosen the threshold parameters a_0 according to the dielectric constants in the Resta model. The threshold parameters a_0 are 0.4/5, 0.4/10 and 0.4/15 accordingly.

TABLE II: The number of convergence steps in the MoS_2 slab systems.

Precondition model	10 layer MoS_2	20 layer MoS_2
Original Kerker	38	52
Resta($\varepsilon(0) = 5$)	25	26
Resta($\varepsilon(0) = 10$)	30	31
Resta($\varepsilon(0) = 15$)	32	32
Modified Kerker ($a_0 = 0.4/5$)	27	27
Modified Kerker ($a_0 = 0.4/10$)	28	32
Modified Kerker ($a_0 = 0.4/15$)	28	32

We further plot the convergence of energies between three preconditioning model in Fig. 2. For the modified Kerker model and the Resta model, we choose the results from those with dielectric constant of 10. The first 5 steps use the blocked Davison scheme thus we plot the energy versus steps from the 6th step.

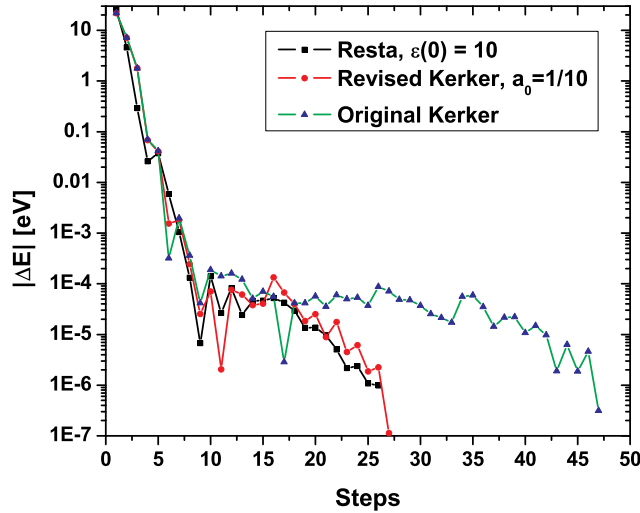


FIG. 2: (color online) The convergence of energies in 20 layer MoS_2 correponding to different preconditioning models.

From Table II and Fig. 2, it is clear that the Resta model and the modified Kerker model

converge the energy faster than the original Kerker scheme, since the MoS₂ slab systems are insulating in nature. These two models give a correct behavior of the incomplete screening effect for insulators at small \mathbf{q} . In addition, using 5, 10 or 15 for the static dielectric constant gives similar results. Therefore, the convergence speed is not that sensitive to the value of static dielectric constant and corresponding parameters.

C. Si slab: the insulating system containing defect states

Even though Resta preconditioner seems to be more appropriate for the insulating systems based on the previous example, we want to further show that this is not the case for the "nominal" insulating systems but containing defect states crossing the Fermi level. A 96 layer Si slab has been constructed with the {111} orientation and a cell parameter of 175 Å along z direction. Both the top and bottom Si surfaces have one dangling bond due to the creation of the surface. A $6 \times 6 \times 1$ k-point grid has been used to sample the Brillouin zone. The cutoff energy is 320 eV. The dielectric constant of bulk Si is about 12. The screening length R_s is 4.2 Å and the q_0 is chosen as 1.1 Å⁻¹, in accord with Resta's parameterizations [24]. As in the case of MoS₂, we compare the convergence speed between the three preconditioning models. The calculated results are shown in Table III.

TABLE III: The number of convergence steps in the original and H-passivated Si slab system.

Preconditioning model	Original Si slab	H-passivated Si slab
Original Kerker	40	46
Modified Kerker ($a_0 = 0.4/12$)	52	29
Resta	47	30

In this case, the original Kerker preconditioner offers the fastest convergence compared with the rest two, which goes against with the conclusion from the previous section. Why is the convergence behavior of the Si slab different from the MoS₂ slab? After careful inspection, we have found that it is the surface states of the Si slab that deviate the system from a "perfect" insulating system.

To better illustrate this, the density of states (DOS) of the Si slab and the corresponding partial charge density distribution of these states have been plotted in Fig. 3(a). We can

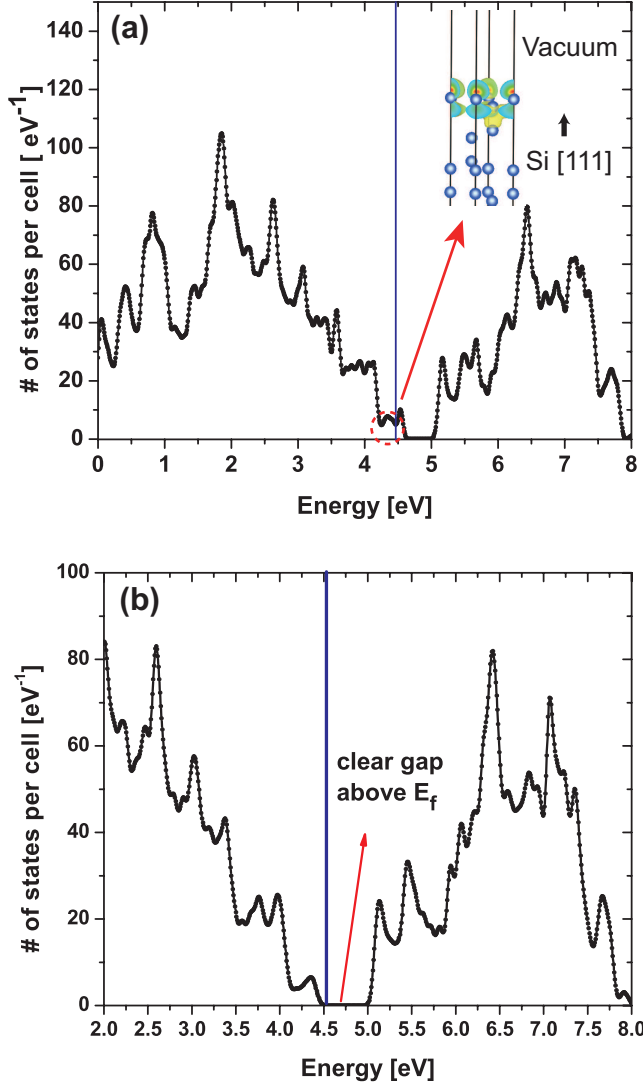


FIG. 3: (color online) (a) The DOS of the 96-atom Si slab. The vertical blue line indicates the Fermi level. The states right below the Fermi level are the surface states, as shown by the partial charge density plot. The bottom surface is identical to the top surface thus only one is shown. (b) The DOS of the Si slab with H passivation (96 layer of Si with 2 H passivation layer on the top and bottom Si surfaces). The added H layers remove the surface states: a clear band gap now occurs right above Fermi level.

see that the creation of the surface introduces defect states right at the Fermi level. The presence of these states drives the system away from a "perfect" insulating system, since there is now allowable states right above the Fermi level. This essential difference makes the preconditioning models for insulators less effective in the Si slab system. In our previous

case, since the MoS_2 is a natural layered material, it will not introduce surface states through creating slabs from the bulk.

To further prove our idea, we passivate the Si surface states through covering the surface by H atoms. Now the system contains 96 layer of Si with 2 extra layer of H covering the top and bottom Si surfaces. The calculation parameters are kept same as the previous case. The convergence speed versus different preconditioning models is also shown in the Table III. Now the trend is consistent with what we have seen in the case of MoS_2 : the modified Kerker (29 steps) and Resta models (30 steps) works better than the original Kerker model (46 steps). Indeed the extra H layers have passivated the dangling bonds on the Si surfaces and removed the surface states. This is clearly shown by the DOS of the H passivated Si slab in Fig. 3(b).

Given this, the modified Kerker preconditioner and Resta preconditioner are better suited for the "prefect" insulating systems. However, introducing metal-like states crossing the Fermi level from defects would render these preconditioning models much less effective.

D. Au- MoS_2 : the metal-insulator hybrid system

Finally we want to discuss the case of metal-insulator hybrid systems. The example system used here is Au- MoS_2 contact systems that combine multiple layers of Au in $\{111\}$ orientation and multiple layers of MoS_2 . The Au layers and MoS_2 layers are in close contact, separated by a distance of the covalent bond length. Such structural models have been studied using DFT calculations to understand the surface, interface and contact properties of Au- MoS_2 epitaxial systems [40–42]. The Au- MoS_2 contact configuration is similar to the $\{111\}$ orientation configuration in Ref. [41]. But for the purpose of examining the performance of the preconditioning models, we have constructed slab systems that are much thicker.

Au- MoS_2 slabs with different fraction of Au and MoS_2 have been created. These slab systems all share same cell parameters and nearly same slab thicknesses and total number of atoms. The total length of the cell is 160 Å with ~ 25 Å vacuum layer and ~ 135 Å Au- MoS_2 slab. The total number of atoms is about 65 with slight variation in different slabs. We use the following notation to label slabs with different fraction of Au and MoS_2 : X Au + Y MoS_2 means we have X layer of Au and Y layer of MoS_2 in the slab. The

total number of atoms is $X + 3Y$ since each MoS_2 contains 3 layer of atom. A $6 \times 6 \times 1$ k-point grid is used to sample the Brillouin zone. The cutoff energy is 450 eV. Here we only test the Kerker preconditioner since Resta model is no longer appropriate to describe $\text{Au}-\text{MoS}_2$ hybrid systems. We would like to seek for the optimized parameterization scheme under the Kerker preconditioning model. As will be shown later, it is possible to achieve fast convergence of such highly inhomogeneous systems under the Kerker preconditioning model, even though the model is based on the homogeneous electron gas.

There are two parameters in the modified Kerker preconditioner to adjust: a_0 and k_{TF} , according to Eqs. (45) and (55). Since these two parameters are describing the effectiveness of the screening from different perspective, we will be only adjusting one parameter while keep the other fixed.

Firstly, based on previous discussion, a_0 is related to the static dielectric constant. For such hybrid systems, we could estimate the upper and lower bound of a_0 . Consider two limits: if the system is full of Au, then a_0 should be set to 0, to go back to the original Kerker scheme; If the system is solely MoS_2 , then a_0 can be set to 0.4/10, as illustrated in the previous section. Actually, we could improve the estimation of lower bound: the mixing of the charge density is done in the reciprocal space and the charge component of the smallest \mathbf{q} is $\frac{2\pi}{L}$, where L is the cell parameter along z . Generally, using any a_0 value smaller than $\alpha \frac{\mathbf{q}^2}{\mathbf{q}^2 + k_{TF}^2}$ is equivalent to setting a_0 to 0. In the case of $\text{Au}-\text{MoS}_2$, L is 160 Å and the minimal effective a_0 is about 6×10^{-4} . However, finding the optimized a_0 in this range is rather difficult. This is because the hybrid system is a highly inhomogeneous system with different parts having distinct dielectric responses. The average static dielectric constant is ill defined than those in the insulating systems. Therefore we perform calculations with various a_0 values between the upper and lower bound (more uniform on the log scale). We note that the k_{TF} is kept to 1 Å⁻¹ in these calculations. The convergence steps versus different threshold parameters a_0 are listed in the Table IV.

From Table IV, we can see that the convergence steps can be less than 35 steps for all $\text{Au}-\text{MoS}_2$ slab systems. Most of the optimized a_0 fall into a region between 3E-3 and 1E-3. However, for the cases of 43 (layer) Au + 6 (layer) MoS_2 and 11 Au + 18 MoS_2 , the original Kerker scheme gives the fastest convergence. Larger a_0 generally results in much worse convergence speed: more than 70 steps for 6E-3 and 1E-2. On the other hand, reduce a_0 close to original Kerker scheme also increases the convergence steps in many cases, but

TABLE IV: The convergence speed in Au-MoS₂ hybrid systems versus threshold parameter a_0 .

Au-MoS ₂ systems	1E-2 ^a	6E-3	3E-3	2E-3	1E-3	8E-4	Original Kerker
43 Au + 6 MoS ₂	88	87	47	43	50	47	<u>34</u> ^b
27 Au + 12 MoS ₂	76	66	45	<u>32</u>	34	50	49
16 Au + 16 MoS ₂	75	82	39	<u>30</u>	34	45	43
11 Au + 18 MoS ₂	72	103	<u>32</u>	33	<u>32</u>	38	<u>32</u>
5 Au + 20 MoS ₂	99	47	33	40	<u>32</u>	39	47
3 Au + 21 MoS ₂	93	55	<u>31</u>	32	<u>31</u>	33	37
1 Au + 22 MoS ₂	39	39	<u>28</u>	40	39	39	37

^a a_0 larger than 1E-2 generally results in very bad convergence or even divergence. Thus we do not list those results.

^bThe fastest convergence is shown in bold and underlined to be distinguished from the rest.

still leads to acceptable convergence speed. Generally the number of steps is below 50 and in some cases the original Kerker scheme gives relatively fast convergence. Based on the numerical results, it is hard to summarize a clear rule for optimizing a_0 . It seems that the optimized a_0 falls into a narrow region. However, being slightly outside this region, especially a larger a_0 , leads to much worse convergence speed. On the other hand, the original Kerker scheme can act as a safe choice.

Now we discuss adjusting the k_{TF} . According to Eq. (48), k_{TF} is related to the number of electrons that can actively participate in the screening. Starting from the system of solely Au, increasing the proportion of MoS₂ part means a reduction in the number of "free" electrons for screening, and resulting in a decreasing value of k_{TF} . For solely Au slab, the value of k_{TF} is 1 Å⁻¹. Replacing a fraction, say $1 - f$, of the Au slab with MoS₂, reduces the number of free electrons n to fn since the MoS₂ makes no contributions to the screening electrons. Therefore, the k_{TF} for the hybrid system can be calculated as $k_{TF} \times f^{1/6}$, according to Eq. (48). For example, in the 27 Au + 12 MoS₂ system, there are total 63 atoms in the system. Thus the Au fraction is 27/63 and the corresponding k_{TF} is given by $(\frac{27}{63})^{(1/6)} \sim 0.87$. We have checked the convergence speed through parameterizing the k_{TF} in this way. The results are listed in Table V together with the results from the optimized a_0 and original Kerker scheme from Table IV.

TABLE V: The convergence speed in Au-MoS₂ hybrid systems versus k_{TF} and a_0 .

Au-MoS ₂ systems	optimized a_0	original Kerker	adjusting k_{TF} ^a
43 Au + 6 MoS ₂	34	34	33 (0.94)
27 Au + 12 MoS ₂	32	49	29 (0.87)
16 Au + 16 MoS ₂	30	43	41 (0.8)
11 Au + 18 MoS ₂	32	32	31 (0.74)
5 Au + 20 MoS ₂	33	47	34 (0.65)
3 Au + 21 MoS ₂	31	37	45 (0.6)
1 Au + 22 MoS ₂	28	37	22 (0.5)

^aThe estimated values of k_{TF} are shown in the parenthesis.

Adjusting k_{TF} in the way described above indeed offer the fastest convergence in many cases, compared with scanning the a_0 between the upper and lower bound. In the 16 Au + 16 MoS₂ system, adjusting k_{TF} offers slower convergence compared that from the optimized a_0 but slightly fast compared with the original Kerker scheme. Only in the 3 Au + 21 MoS₂ system, adjusting k_{TF} gives the slowest convergence compared with the rest two. In addition, with small adjustment near the calculated k_{TF} , these two systems can also achieve the fastest convergence. For the 16 Au + 16 MoS₂ system, changing k_{TF} from initial value 0.8 to 0.85, one can reach the convergence at 31st step. For the 3 Au + 21 MoS₂ system, changing k_{TF} from 0.6 to either 0.55 and 0.65, the convergence steps become 31 and 32, respectively. We conclude that adjusting k_{TF} in such way could either give the very fast convergence or be a good initial guess of further optimizing the k_{TF} . We further note that adopting this parameterization scheme requires *a priori* knowledge of the system. The parameterization scheme for systems without enough *a priori* knowledge will be discussed in the next section.

V. FURTHER DISCUSSIONS

We would like to address few important points before we reach the final conclusions:

1. The Thomas-Fermi screening model and modified Kerker preconditioner

It is well known that the Thomas-Fermi screening model is built on the homogeneous

electron gas and the Kerker preconditioner is rooted in the Thomas-Fermi screening model. However, based on the numerical examples, we can see that with some simple (but physically meaningful) modifications, the Kerker preconditioner can be applied to a wide range of materials, most of which are no way near the free electron gas system, such as the insulating systems and the metal-insulator contact systems. Then what is the merit in the modifications of the Kerker preconditioner? According to our experience, the description of the long-range screening behavior is crucial to reach fast convergence. While in the modified Kerker scheme, it is possible to capture the essence of this behavior: the original Kerker scheme naturally suppress the \mathbf{q}^2 divergence at $\mathbf{q} \rightarrow 0$ limit in the metallic system; The incomplete screening effect in the insulating systems is captured by the threshold parameter a_0 ; As for the metal-insulator contact system, the long-range screening effect is characterized by the number of effective electrons that participate in the screening. This number is represented by the parameter k_{TF} . Our numerical examples indeed prove the effectiveness of the modified Kerker preconditioner: converging a long slab system (with more than 60 layer and more than 15 nm long in cell parameter) to relatively high accuracy in about 30 steps is significant for practical applications.

2. *A posteriori* indicator of charge sloshing

Previously, we focus on the discussion of situations when we have enough *a priori* knowledge. In many practical cases, however, we may not know enough about the system before doing the calculation. Now it is rather difficult to optimize parameters in Kerker preconditioner. With one step back, we can still monitor if the charge sloshing occurs during the SCF iterations through an *a posteriori* indicator. Theoretically, the charge sloshing is indicated by the spectrum of the matrix JP or its inverse $(JP)^{-1}$ from Eq. (6). Practically, we compute the eigenvalues of $P^{-1}H_m$ instead of $(JP)^{-1}$. The preconditioning matrix P is a symmetric positive definite with the Kerker scheme or our modified version. The matrix H_m updated by (27) satisfies the constraint condition in Eq. (24):

$$H_m Y_{m-1} = -S_{m-1}. \quad (57)$$

Assuming the vectors \mathbf{x}_{m-i} all sufficiently close to the solution of Eq. (1), we have

$$J^{-1}Y_{m-1} \approx -S_{m-1}. \quad (58)$$

Comparing Eq. (57) with Eq. (58), we find that H_m is almost the best approximation of the inverse Jacobian J^{-1} in the subspace spanned by Y_{m-1} . Consequently we calculate

the eigenvalues of $P^{-1}H_m$ in this subspace by solving the following generalized eigenvalue problem:

$$Y_{m-1}^T H_m Y_{m-1} \mathbf{u}_i = \lambda_i Y_{m-1}^T P Y_{m-1} \mathbf{u}_i. \quad (59)$$

In implementation, we shift Eq. (59) as like

$$Y_{m-1}^T (H_m - P) Y_{m-1} \mathbf{u}_i = (\lambda_i - 1) Y_{m-1}^T P Y_{m-1} \mathbf{u}_i. \quad (60)$$

Note that it takes extra small computational overhead on solving Eq. (60) since $(H_m - P)Y_{m-1} = -(S_{m-1} + H_1 Y_{m-1})$ has been calculated in Pulay's update and the dimension of Eq. (60) is less than 50 in our codes.

As far as we know, Kresse and Furthmüller [3] propose similar formulations as Eqs.(59) and (60) to discuss the spectrum range for insulators and open-shell transition metals of different sizes. Instead of examining the range of spectrum, we extract the minimal module of the eigenvalues from Eq. (59). This value is the *a posteriori* indicator to show whether the preconditioner have suppressed charge sloshing or not. If charge sloshing occurs, the *a posteriori* indicator would on the order of 0.01 due to the divergence of the dielectric function. In this case, we suggest users to terminate the task and switch to original Kerker scheme.

We demonstrate the *a posteriori* indicator in calculations of the 3 Au + 21 MoS₂ system. The energy convergence and the minimal eigenvalue of the Jacobian matrix during the SCF calculation under different a_0 are plotted in Fig. 4. Without any previous experience, one would guess the 3 Au + 21 MoS₂ system should be close to solely MoS₂ system. In this sense, the threshold parameter a_0 should be set to 0.4/10 = 4E-2. As shown in Fig 4, this leads to very bad convergence. The *a posteriori* indicator we defined stay at the order of 1E-2, indicating an incomplete suppression of the charge sloshing. To improve this, we use a much smaller a_0 (3E-4) and redo the calculation. Note that the smallest effective a_0 is about 6E-4 according to our previous discussion, setting a_0 to 3E-4 is equivalent to original Kerker scheme. Now the convergence is reached at 37th step and the *a posteriori* indicator stay at the order of 1, suggesting a good suppression of charge sloshing.

We have also made some efforts in realizing the self-adaptive parameterizations, in which the algorithm updates the threshold parameter during the SCF calculation. However, it seems the change of the threshold parameter inside a SCF loop wound render the Pulay

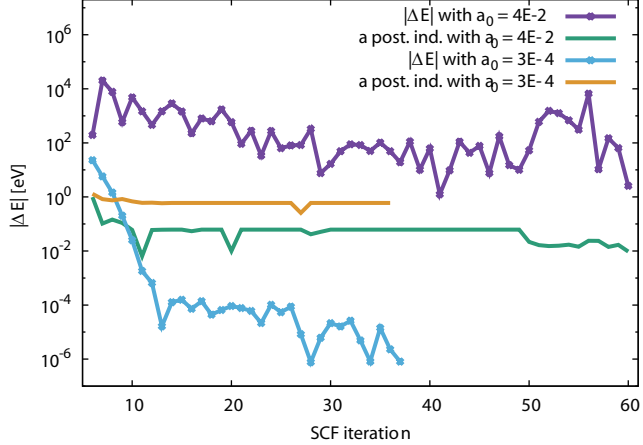


FIG. 4: (color online) The energy convergence and the minimal eigenvalue of the Jacobian matrix versus convergence step under different a_0 are shown. The threshold parameters for two SCF calculations are 3E-4 and 4E-2, respectively.

mixing scheme much more unstable since the results used to built the next input are from old threshold parameter.

3. General parameterization strategy

Now, we present a general strategy for setting the parameters in the modified Kerker preconditioner for the calculations of large systems. The strategy is summarized in Table VI. Here, we comment few things on this general strategy:

TABLE VI: The general parameterization strategy for large dimension systems.

	Metal	Insulator	Metal-Insulator hybrid
With <i>a priori</i> knowledge	Original Kerker or $a_0 = 0$	$a_0 = \alpha/\varepsilon(0)$ or $a_0 = \alpha/10$	Set $k_{TF} \approx f^{1/6}$ f : fraction of metal
No <i>a priori</i> knowledge	(1) Set $a_0 \approx \alpha \frac{q_{min}^2}{q_{min}^2 + k_{TF}^2}$ ^a or the original Kerker scheme: $a_0 = 0$	(2) Set $a_0 = \alpha/10$, monitor the smallest eigenvalue of $(JP)^{-1}$ in SCF iterations. If charge sloshing occurs, switch to (1)	

^aSpecifically, "≈" means 1 ∼ 2 times the value from the right side. q_{min} is the smallest reciprocal wave vector.

(1) For the calculation of insulator, we can use a default value of 10 if the static dielectric constant is unknown. Because the static dielectric constant for most insulators fall into the

range between $5 \sim 15$. According to our experience, the convergence is not that sensitive to the value of static dielectric constant. Therefore, we expect the default setting of static dielectric constant can also help to achieve fast convergence in many insulating systems.

(2) In the case of metal-insulator hybrid, we are talking about situations that metal region and insulator region are spatially separated and well defined, such as the metal-insulator contact systems illustrated in this paper. A fine mixing of them on the scale of atomic distance does not fall into this category. Such situation should be treated as a system without *a priori* knowledge unless further information can be founded.

(3) When there is no *a priori* knowledge of the system, either (1) or (2) in Table VI can be used. Strategy (1) is very close to the original Kerker preconditioner. For the hybrid system, slightly increasing a_0 from the lower bound ($\alpha \frac{q_{min}^2}{q_{min}^2 + k_{TF}^2}$) often improve the convergence speed. Thus we also suggest it for systems without *a priori* knowledge. Strategy (1) will work well for the metallic systems and has acceptable performance on the insulating and metal-insulator hybrid systems. This is a rather safe choice. On the other hand, strategy (2) would better converge the calculations of insulator at the risks of worsening the convergence in metallic systems. However, an *a posteriori* indicator is introduced to monitor the SCF loop. If charge sloshing occurs, one could redo the calculation with reduced value of a_0 . The use of *a posteriori* indicator has been demonstrated in the last point.

VI. CONCLUSIONS

In sum, we have proposed that the Kerker scheme with physically meaningful modifications can be generalized to improve the convergence for metallic, insulating and metal-insulator hybrid systems. The modifications are taken in two aspects: the threshold parameter a_0 characterize the screening behavior of insulators at long-range limit thus helps to accommodate the insulating systems; The k_{TF} represents the effective number of metal-like electrons near the Fermi level and can be used to speed up the convergence of metal-insulator hybrid systems. From our numerical examples, the Kerker preconditioner is effective and efficient for the SCF calculations of inhomogeneous systems. We also provide a general strategy to parameterize the modified Kerker scheme to improve the efficiency in either *a priori* or *a posteriori* way.

APPENDIX

Now we prove Eq. (26) is the solution to the constraint optimization problem Eq. (24). First we prove the following lemma.

Lemma 1. *Let $X \in \mathbb{C}^{m \times n}$, $A \in \mathbb{C}^{n \times p}$, $B \in \mathbb{C}^{m \times p}$, and assume that A has full column rank. Denote the Moore-Penrose pseudoinverse of A by A^\dagger with $A = (A^H A)^{-1} A^H$. If $XA = B$ is satisfiable, and the matrix $Z \equiv BA^\dagger$, then it holds that*

$$\|Z\|_F \leq \|X\|_F \quad (61)$$

Proof. Let $Q \equiv AA^\dagger$. Then it follows that $Q^H = Q$ and $ZQ = Z$. Thus we have

$$\begin{aligned} (X - Z, Z)_F &\equiv \text{tr}[(X - Z)Z^H] \\ &= \text{tr}[(X - Z)(ZQ)^H] \\ &= \text{tr}[(X - Z)Q^HZ^H] \\ &= \text{tr}[(X - Z)QZ^H] \\ &= \text{tr}[(XAA^\dagger - ZQ)Z^H] \\ &= \text{tr}[(BA^\dagger - Z)Z^H] \\ &= 0 \end{aligned} \quad (62)$$

Note that Eq. (63) is an inner product corresponding to the Frobenius norm $\|\cdot\|_F$. Hence

$$\begin{aligned} \|X\|_F^2 &= \|X - Z\|_F^2 + 2(X - Z, Z)_F + \|Z\|_F^2 \\ &= \|X - Z\|_F^2 + \|Z\|_F^2 \\ &\geq \|Z\|_F^2 \end{aligned}$$

with equality if and only if $X = Z$. \square

Let $H' \equiv H - H_{m-1}$. Thus the optimization problem (24) can be replaced by its equivalent one

$$\begin{cases} \min_{H'} \|H'\|_F^2 \\ \text{s.t. } H'Y_{m-1} = -(S_{m-1} + H_{m-1}Y_{m-1}), \end{cases} \quad (63)$$

It follows from Lemma 1 that the solution to the problem Eq. (63) is

$$H' = -(S_{m-1} + H_{m-1}Y_{m-1}) (Y_{m-1}^T Y_{m-1})^{-1} Y_{m-1}^T. \quad (64)$$

Therefore the solution to the problem (24) is

$$H = H_{m-1} - (S_{m-1} + H_{m-1}Y_{m-1}) (Y_{m-1}^T Y_{m-1})^{-1} Y_{m-1}^T. \quad (65)$$

This work was partially supported by the National Key Research and Development Program of China under Grant 2016YFB0201204, the National Science Foundation of China under Grants 11501039 and 91430218.

- [1] P. Hohenberg and W. Kohn, Phys. Rev. **136**, B864 (1964), URL <https://link.aps.org/doi/10.1103/PhysRev.136.B864>.
- [2] W. Kohn and L. J. Sham, Phys. Rev. **140**, A1133 (1965), URL <https://link.aps.org/doi/10.1103/PhysRev.140.A1133>.
- [3] G. Kresse and J. Furthmüller, Phys. Rev. B **54**, 11169 (1996), URL <https://link.aps.org/doi/10.1103/PhysRevB.54.11169>.
- [4] G. Kresse and J. Furthmüller, Computational Materials Science **6**, 15 (1996), ISSN 0927-0256, URL <http://www.sciencedirect.com/science/article/pii/0927025696000080>.
- [5] J. F. Annett, Computational Materials Science **4**, 23 (1995), ISSN 0927-0256, URL <http://www.sciencedirect.com/science/article/pii/0927025694000133>.
- [6] L. D. Marks and D. R. Luke, Phys. Rev. B **78**, 075114 (2008), URL <https://link.aps.org/doi/10.1103/PhysRevB.78.075114>.
- [7] P. J. Hasnip, K. Refson, M. I. J. Probert, J. R. Yates, S. J. Clark, and C. J. Pickard, Philosophical Transactions of the Royal Society of London A: Mathematical, Physical and Engineering Sciences **372** (2014), ISSN 1364-503X, <http://rsta.royalsocietypublishing.org/content/372/2011/20130270.full.pdf>, URL <http://rsta.royalsocietypublishing.org/content/372/2011/20130270>.
- [8] J. K. Norskov, F. Abild-Pedersen, F. Studt, and T. Bligaard, Proceedings of the National Academy of Sciences **108**, 937 (2011), <http://www.pnas.org/content/108/3/937.full.pdf>, URL <http://www.pnas.org/content/108/3/937.abstract>.
- [9] C. G. Van de Walle and R. M. Martin, Phys. Rev. B **34**, 5621 (1986), URL <https://link.aps.org/doi/10.1103/PhysRevB.34.5621>.

[10] P. Pulay, Chemical Physics Letters **73**, 393 (1980), ISSN 0009-2614, URL <http://www.sciencedirect.com/science/article/pii/0009261480803964>.

[11] C. G. Broyden, Math. Comp. **19**, 577 (1965).

[12] G. P. Kerker, Phys. Rev. B **23**, 3082 (1981), URL <https://link.aps.org/doi/10.1103/PhysRevB.23.3082>.

[13] D. Raczkowski, A. Canning, and L. W. Wang, Phys. Rev. B **64**, 121101 (2001), URL <https://link.aps.org/doi/10.1103/PhysRevB.64.121101>.

[14] D. Vanderbilt and S. G. Louie, Phys. Rev. B **30**, 6118 (1984), URL <https://link.aps.org/doi/10.1103/PhysRevB.30.6118>.

[15] Y. Shiihara, O. Kuwazuru, and N. Yoshikawa, Modelling and Simulation in Materials Science and Engineering **16**, 035004 (2008), URL <http://stacks.iop.org/0965-0393/16/i=3/a=035004>.

[16] L. Lin and C. Yang, SIAM Journal on Scientific Computing **35**, S277 (2013), <http://dx.doi.org/10.1137/120880604>, URL <http://dx.doi.org/10.1137/120880604>.

[17] K.-M. Ho, J. Ihm, and J. D. Joannopoulos, Phys. Rev. B **25**, 4260 (1982), URL <https://link.aps.org/doi/10.1103/PhysRevB.25.4260>.

[18] A. Sawamura and M. Kohyama, Mater. Trans. **45**, 1422 (2004).

[19] P.-M. Anglade and X. Gonze, Phys. Rev. B **78**, 045126 (2008), URL <https://link.aps.org/doi/10.1103/PhysRevB.78.045126>.

[20] R. B. R and R. Ahlrichs, J. Chem. Phys. **104**, 9047 (1996).

[21] D. D. Johnson, Phys. Rev. B **38**, 3082 (1988).

[22] H. Fang and Y. Saad, Numer. Linear. Algebra Appl. **16**, 197 (2009).

[23] L. LANDAU and E. LIFSHITZ, *Electrodynamics of Continuous Media (Second Edition Revised and Enlarged)*, vol. 8 (Pergamon, 1984), second edition revised and enlarged ed.

[24] R. Resta, Phys. Rev. B **16**, 2717 (1977), URL <https://link.aps.org/doi/10.1103/PhysRevB.16.2717>.

[25] D. R. Penn, Phys. Rev. **128**, 2093 (1962), URL <https://link.aps.org/doi/10.1103/PhysRev.128.2093>.

[26] G. SRINIVASAN, Phys. Rev. **178**, 1244 (1969), URL <https://link.aps.org/doi/10.1103/PhysRev.178.1244>.

[27] J. P. Walter and M. L. Cohen, Phys. Rev. B **2**, 1821 (1970), URL <https://link.aps.org/doi/10.1103/PhysRevB.2.1821>.

[28] X. S. Shajan and C. Mahadevan, Crystal Research and Technology **27**, 253 (1992), ISSN

1521-4079, URL <http://dx.doi.org/10.1002/crat.2170270217>.

[29] P. K. W. Vinsome and D. Richardson, Journal of Physics C: Solid State Physics **4**, 2650 (1971), URL <http://stacks.iop.org/0022-3719/4/i=16/a=030>.

[30] J. Fang, X. Gao, H. Song, and H. Wang, The Journal of Chemical Physics **144**, 244103 (2016), <http://dx.doi.org/10.1063/1.4954234>, URL <http://dx.doi.org/10.1063/1.4954234>.

[31] X. Gao, Z. Mo, J. Fang, H. Song, and H. Wang, Computer Physics Communications **211**, 54 (2017), ISSN 0010-4655, high Performance Computing for Advanced Modeling and Simulation of Materials, URL <http://www.sciencedirect.com/science/article/pii/S0010465516301837>.

[32] Z. Mo, A. Zhang, X. Cao, Q. Liu, X. Xu, H. An, W. Pei, and S. Zhu, Frontiers of Computer Science in China **4**, 480 (2010), ISSN 1673-7466, URL <http://dx.doi.org/10.1007/s11704-010-0120-5>.

[33] J. P. Perdew, K. Burke, and M. Ernzerhof, Phys. Rev. Lett. **77**, 3865 (1996), URL <http://link.aps.org/doi/10.1103/PhysRevLett.77.3865>.

[34] G. Kresse and D. Joubert, Phys. Rev. B **59**, 1758 (1999), URL <http://link.aps.org/doi/10.1103/PhysRevB.59.1758>.

[35] B. Liu, in *Numerical Algorithms in Chemistry: Algebraic Methods*, edited by E. Moler and I. Shavitt (Lawrence Berkley Lab. Univ. of California, 1978), p. 49.

[36] A. Molina-Sánchez and L. Wirtz, Phys. Rev. B **84**, 155413 (2011), URL <https://link.aps.org/doi/10.1103/PhysRevB.84.155413>.

[37] T. Cheiwchanchamnangij and W. R. L. Lambrecht, Phys. Rev. B **85**, 205302 (2012), URL <https://link.aps.org/doi/10.1103/PhysRevB.85.205302>.

[38] L. Liang and V. Meunier, Nanoscale **6**, 5394 (2014), URL <http://dx.doi.org/10.1039/C3NR06906K>.

[39] N. Saigal, V. Sugunakar, and S. Ghosh, Applied Physics Letters **108**, 132105 (2016), <http://dx.doi.org/10.1063/1.4945047>, URL <http://dx.doi.org/10.1063/1.4945047>.

[40] I. Popov, G. Seifert, and D. Tománek, Phys. Rev. Lett. **108**, 156802 (2012), URL <http://link.aps.org/doi/10.1103/PhysRevLett.108.156802>.

[41] Y. Zhou, D. Kiriya, E. E. Haller, J. W. Ager, A. Javey, and D. C. Chrzan, Phys. Rev. B **93**, 054106 (2016), URL <https://link.aps.org/doi/10.1103/PhysRevB.93.054106>.

[42] J. Kang, W. Liu, D. Sarkar, D. Jena, and K. Banerjee, Phys. Rev. X **4**, 031005 (2014), URL

<https://link.aps.org/doi/10.1103/PhysRevX.4.031005>.

[43] Strictly speaking, the ε derived here is respect to the potential. However, under the condition of homogeneous system, the potential dielectric response function and charge dielectric response function are same. This is because the χ in Eq. (15) becomes diagonalized thus the product of $\chi \cdot U$ equals to $U \cdot \chi$.